Estuarine, Coastal and Shelf Science 244 (2020) 106941

Contents lists available at ScienceDirect

Estuarine, Coastal and Shelf Science

journal homepage: http://www.elsevier.com/locate/ecss

Estuarine tidal response to sea level rise: The significance of entrance restriction

Danial Khojasteh [a,*], Steve Hottinger [a,b], Stefan Felder [a], Giovanni De Cesare [b], Valentin Heimhuber [a], David J. Hanslow [c], William Glamore [a]

[a] Water Research Laboratory, School of Civil and Environmental Engineering, UNSW, Sydney, NSW, Australia
[b] Platform of Hydraulic Constructions (PL-LCH), Ecole Polytechnique Fédérale de Lausanne (EPFL), Lausanne, Switzerland
[c] Science, Economics and Insights Division, Department of Planning, Industry and Environment, NSW Government, Locked Bag 1002 Dangar, NSW 2309, Australia

ARTICLE INFO

Keywords:
Estuarine hydrodynamics
Tidal asymmetry
Resonance
Idealised method
Ensemble modelling
Cluster analysis

ABSTRACT

Estuarine environments, as dynamic low-lying transition zones between rivers and the open sea, are vulnerable to sea level rise (SLR). To evaluate the potential impacts of SLR on estuarine responses, it is necessary to examine the altered tidal dynamics, including changes in tidal amplification, dampening, reflection (resonance), and deformation. Moving beyond commonly used static approaches, this study uses a large ensemble of idealised estuarine hydrodynamic models to analyse changes in tidal range, tidal prism, phase lag, tidal current velocity, and tidal asymmetry of restricted estuaries of varying size, entrance configuration and tidal forcing as well as three SLR scenarios. For the first time in estuarine SLR studies, data analysis and clustering approaches were employed to determine the key variables governing estuarine hydrodynamics under SLR. The results indicate that the hydrodynamics of restricted estuaries examined in this study are primarily governed by tidal forcing at the entrance and the estuarine length. In addition, SLR increases the average water depth and alters the nodal point location in a seaward direction, thereby significantly affecting tidal wave propagation patterns and reducing the degree of flood domination. In estuaries with restricted entrances, tidal range diminishes drastically in the restricted zone by 20–60%, and the maximum tidal current velocity is higher in the restricted part but lower in the upstream part compared to unrestricted estuaries. For estuary types examined, inundation extent under SLR will likely be greater than the extent expected through simply adjusting existing water levels upwards. The findings also underline that an engineered entrance restriction could regulate tidal wave propagation within an estuary to offset SLR induced tidal range amplification. However, this may pose additional management challenges.

1. Introduction

Estuaries are among the most productive ecosystems worldwide, supporting large communities of plants and animals as well as promoting economic, social, and environmental activities. 21 out of the 30 largest cities in the world are located adjacent to estuaries. Globally, sea level rise (SLR) projections indicate a likely rise of between 0.29 and 1.10 m for lower and upper Representative Concentration Pathways by 2100 relative to 1986–2005 (Oppenheimer et al., 2019). Above the likely range, SLR of 2 m or more may be possible due to the uncertainties associated with the instability of the Antarctic and Greenland ice-sheets (Bamber et al., 2019; DeConto and Pollard, 2016; Horton et al., 2020; Kulp and Strauss, 2019). The USA National Oceanic and Atmospheric Administration also reported SLR of up to 2–2.5 m by the end of this century (Sweet et al., 2017).

As estuaries are transition zones between rivers and the open sea, and are typically located in very low-lying areas, they are highly susceptible to accelerating SLR (Grenfell et al., 2016; Hanslow et al., 2018; Passeri et al., 2015c). The potential impacts of SLR in estuaries include more frequent inundation, shoreline recession, failure of sewerage and drainage systems, drowning of intertidal wetlands, and possibly drastic changes in the hydrodynamic regime (Bergillos et al., 2019; Hanslow

* Corresponding author.
E-mail addresses: danial.khojasteh@unsw.edu.au (D. Khojasteh), steve.hottinger@epfl.ch (S. Hottinger), s.felder@unsw.edu.au (S. Felder), giovanni.decesare@epfl.ch (G. De Cesare), v.heimhuber@unsw.edu.au (V. Heimhuber), david.hanslow@environment.nsw.gov.au (D.J. Hanslow), w.glamore@wrl.unsw.edu.au (W. Glamore).

https://doi.org/10.1016/j.ecss.2020.106941
Received 26 April 2020; Received in revised form 14 July 2020; Accepted 24 July 2020
Available online 30 July 2020

et al., 2018; Wiegman et al., 2018; Yuan and Zhu, 2015). To make informed management decisions regarding the potential impacts of SLR in and around estuaries, in-depth knowledge of the altered estuarine hydrodynamics is required.

Approaches to SLR inundation assessments vary from simplistic elevation-based calculations (Chen and McAneney, 2006; Titus and Richman, 2001), sometimes adjusted to allow for variations in ocean tides and storm surges (Strauss et al., 2012) to those based on estuarine gauge data and interpolation (Hanslow et al., 2018; NOAA, 2017) to detailed local studies using hydrodynamic modelling (Lee et al., 2017; Palmer et al., 2019; Passeri et al., 2015b). The elevation-based methods make no allowance for hydrodynamic processes and essentially assume bathtub style drowning of all land below a given water surface elevation. This may either under- or overestimate existing inundation depending on the shape/type of estuary (Hanslow et al., 2018). The interpolation-based approaches use existing gauge data and thus allow for current estuarine processes but are unable to account for any change in tidal processes with SLR. As a result, they cannot fully account for SLR impacts on important phenomena that are well known to affect the propagation of the tidal wave in estuarine settings including tidal dampening, amplification, deformation, and reflection (or resonance) (Anderson et al., 2018; Hoeke et al., 2013; Khojasteh et al., 2019; Melet et al., 2018). Only hydrodynamic modelling is capable of capturing the complex and nonlinear responses of estuarine hydrodynamics to SLR (Moftakhari et al., 2019; Palmer et al., 2019; Rodríguez et al., 2017).

The hydrodynamic regime of an estuary is largely governed by external driving forces including tides, wind, waves, and inflows (riverine and groundwater). In addition to these external forces, the shape and boundary conditions of an estuary (e.g. depth, length, width, entrance configuration, and roughness), fluid properties (e.g. water density and viscosity) and forces directly acting on the water body (density gradients and gravitational forces) determine the hydrodynamics of estuaries (Du et al., 2018; Talke and Jay, 2020).

Estuaries can be classified into two basic types depending on whether the entrance is restricted or not (Fairbridge, 1980), which is determined by the interaction between river inflows, waves and tides (McSweeney et al., 2017). The entrance can be restricted to regulate estuarine water level, tidal prism, salinity distribution and water quality (Hinwood et al., 2012; MacMahan et al., 2014). Many estuaries worldwide have entrances that are periodically changing, shifting from a closing phase, due to the accretion of marine sediment and berm formation, to an opening phase, when there is sufficient water discharging from the catchments into the ocean (McSweeney et al., 2017; Sadat-Noori et al., 2016). These estuaries are globally called by different terms as further discussed by McSweeney et al. (2017) including Intermittently Closed/Open Lakes and Lagoons (ICOLLs), Temporarily Open/Closed Estuaries (TOCEs), bar-built estuaries, and/or seasonally open inlets. Other types of restricted entrances exist in estuaries that have narrow ribbon-shaped entrances where the sides are formed by naturally rising ground or artificial embankments, entrances which are restricted by rocks and form a basin in their middle part, and sedimentary barriers across the mouth (Pye and Blott, 2014). The changes in entrance configuration will likely be altered under SLR as rising sea levels influence the shape and bathymetry of the estuary as well as the propagation patterns of the tidal wave within the estuary (Khojasteh et al., 2019; Leuven et al., 2019; Talke and Jay, 2020). Likewise, any anthropogenic or natural changes to the entrance condition would influence the estuary tidal dynamics (Hinwood and McLean, 2015; McSweeney et al., 2017).

The influence of entrance condition and SLR on the upstream tidal propagation pattern has long been a growing concern to estuarine and coastal engineers. However, this research topic is still subject to a variety of knowledge gaps as most studies have not focused on the estuarine entrance condition (see for example Passeri et al. (2015a), Passeri et al. (2015b), Ross et al. (2017), and Du et al. (2018)). Further, existing estuarine entrance studies have often focused on a specific real-world case study, such as the Snowy River Estuary, Australia (Hinwood and McLean, 2018), Lake Illawarra, Australia (Young et al., 2014), Lakes Macquarie, Wallis, and Wagonga, Australia (Callaghan et al., 2020; Nielsen and Gordon, 2017), Yangshan Deep-water Harbour, China (Guo et al., 2018), Lake Hamanako, Japan (Hinwood et al., 2017), Jamaica, Great South and connected bays, USA (Aretxabaleta et al., 2017), and New River estuary, USA (MacMahan et al., 2014). Most of these studies have examined the estuarine entrance stability, tidal range, and sediment dynamics, leaving other key estuarine parameters and processes such as tidal prism, tidal current velocity, tidal phase, and tidal asymmetry unstudied. Most of these studies have not considered the effect of SLR within a restricted entrance and the resultant changes in hydrodynamics. Therefore, a systematic framework is currently absent to estimate how estuaries of different sizes and entrance configurations will respond to SLR.

To partially address this knowledge gap, this study investigates the combined effect of SLR and entrance restrictions on the tidal dynamics of idealised estuaries, while limitations of the current approach and recommendations for future studies are discussed. This study aims to address the following questions:

(1) How does the entrance condition influence the hydrodynamic response of estuaries under SLR?
(2) Which physical parameters govern the tidal responses of restricted and unrestricted estuaries to SLR?
(3) Are mitigation measures available to reduce SLR impacts on estuaries?

2. Methodology

2.1. Numerical simulations

The hydrodynamic response of prismatic estuaries with restricted entrances to SLR were examined by simulating a large ensemble of idealised estuarine hydrodynamic models (200 simulation cases) of varying length, tidal forcing, and entrance restrictions under 0, 1 and 2 m of SLR. Fig. 1 schematically illustrates an idealised prismatic estuary considered in this study and the applied boundary conditions. Table 1 presents the parameters that were varied across the simulation cases. The values presented in this table can be representatives of some real-world estuaries as highlighted by Bruun and Gerritsen (1960) and FitzGerald et al. (2002) for restriction width, length, and distance from entrance; Arcement and Schneider (1989) for Manning coefficient; and Savenije (2006), Du et al. (2018), and Leuven et al., 2019 for estuarine length, width, and depth. For each case, the model was run for a period of 60 days with a time step of 15 minutes. The outputs were saved at each time step and the results for the initial 10 days were discarded to ensure any startup instabilities were avoided during the initialisation of the model.

It was assumed that the tides at the ocean boundary are driven by the semi-diurnal tidal constituent M_2 with a sinusoidal signal of 12.42 h and applied at the estuary entrance (see Fig. 1). Vertical boundaries were assumed along the riverbank edge to prevent flooding of adjacent areas. This study has solely focused on the implications of SLR on tidal

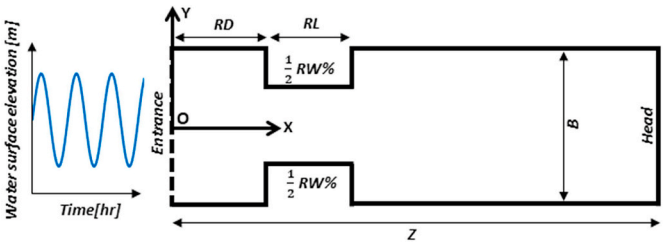

Fig. 1. A schematic top view of an idealised prismatic estuary with a restricted entrance as considered in this study. All symbols are defined in Table 1.

Table 1
Investigated parameters and their value range.

Parameter	Value(s)
Estuary length (Z) [km]	40, 60, 80, 100, 160
Estuary width (B) [km]	1
Estuary depth (h) [m]	5
Restricted width (RW) [%]	0, 10, 20, 30, 40, 50, 60,70, 80, 90
Restriction length (RL) [m]	500
Restriction distance from the entrance (RD) [m]	400
Tidal range (TR) [m]	1, 4
Sea level rise [m]	0, 1, 2
Tidal period (T) [hour]	12.42
Manning coefficient n [s/m$^{1/3}$]	0.03

dynamics and thereby, the effects of freshwater inflows, storm surges, waves and wind were neglected. Geomorphological changes were not considered as they manifest at longer time scales.

A rigid entrance restriction was applied by reducing the entrance cross-section by a desired percentage ($RW \times RL$), starting at $RD = 400$ m. To illustrate, $RW = 50\%$ means that 50% of the entrance cross-section is blocked by reducing 25% from each channel side. Several RWs were tested and it was noted that restricting the entrance by $RW = 40$–50% is a threshold after which tidal response changes significantly. This phenomenon is highlighted in Fig. S1 in the Supplementary Material. As such, most of the results are focused on unrestricted ($RW = 0\%$) and highly restricted ($RW = 80\%$) estuaries.

2.2. Hydrodynamic model and validation

All cases were simulated using the RMA-2 hydrodynamic modelling package (2D - version 8.6) that solves the depth-integrated shallow water equations (Khojasteh et al., 2020) to simulate the water surface elevation and velocities over time and space (Elmoustafa, 2017; King, 2013; King et al., 1997). This model is well-established and widely used for river and estuarine flow modelling (Proudfoot et al., 2018; Rao, 2005). The solver uses the Galerkin finite element method and a modified Crank Nicholson implicit time integration scheme for transient conditions, and as a result, the model is not stability limited by the Courant condition (King et al., 1997). Time steps can be designed to match the rates of variation of depth/velocity in the system. Therefore, this method is powerful in ocean and estuarine applications, as large time steps can be used in conjunction with higher resolutions (King and Norton, 1978; Ye et al., 2016; Zhang et al., 2016). RMA-2 uses horizontal eddy viscosity coefficients for each element to define turbulence characteristics (Rao, 2005). Further, a mesh independency check was undertaken to ensure an optimum mesh density to capture the desired flow characteristics and optimize the computational costs. Based on this analysis, mesh resolutions of 12.5 m and 200 m were chosen at/around the restricted entrance and for the rest of the domain, respectively. The accuracy of the model has been verified and is available in previous works (Hottinger, 2019; Khojasteh et al., 2019).

2.3. Identifying key variables using clustering and data analysis techniques

For all simulated cases, the water surface elevations and flow velocities were extracted every 15 minutes at each node for 50 days, building a large database of flow information. In order to identify the key parameters that control the hydrodynamic response of estuaries to SLR, a clustering technique was used to help maximising insights into this dataset. The reader is referred to the Supplementary Material for further details of the applied clustering method.

3. Results

3.1. Changes in tidal range, tidal prism, and phase lag

Here, the effects of changes in estuarine shape (length and entrance restriction) on the tidal amplification, dampening, deformation, reflection, and resonance under three SLR scenarios are investigated by testing tidal ranges at mouth (TR_0) of 1 and 4 m, and $Z = 40$, 60, 80, 100 and 160 km for restricted and unrestricted channels. The estuarine tidal response is analysed by plotting the normalized tidal range (tidal range at any location along the channel divided by tidal range at the mouth (TR/TR_0)) (Figs. 2 and 3). In these figures, values above the line $TR/TR_0 = 1$ indicate tidal amplification, while values below this line represent tidal dampening.

As shown in Fig. 2, a 20–60% reduction in tidal range occurs over the first kilometre if entrances are restricted by $RW = 80\%$, illustrating the frictional effect and the head loss induced by entrance restriction. This phenomenon is well documented for real-world estuaries where a reduction in entrance cross-sectional area contributes to initial attenuation of tides (Hanslow et al., 2018; Kumbier et al., 2018). Further, SLR increases the tidal ranges of all cases by approximately 10–20% per meter of SLR (averaged along the entire length of the estuary).

In short channels of Fig. 2(a, c) and Fig. 3(a), tides are amplified within the estuary (after the restricted zone) due to the reflection induced from the closed end, which is typical in short estuaries (Savenije, 2006). However, tides are generally dampened in longer estuaries, as in Fig. 2(b, d) and Fig. 3(c), as most of the energy is dissipated through the bed/banks friction. This is in line with the findings of Prandle (2003) who analytically showed that frictional energy losses depend on the tidal range over channel depth ratio (TR/h), with higher ratios demonstrating friction domination in the channel. As a real-world example, friction has been shown to be irrelevant in tidal amplitude distribution of Alfacs Bay (NW Mediterranean Sea) due to the low ratio of TR/h ($\simeq$0.1) (Cerralbo et al., 2014).

In estuaries, tidal resonance occurs when natural frequency of an estuarine system matches the tidal frequency (Le Souëf and Allen, 2014). For a frictionless channel of constant width and depth, a theoretical resonance length exists as $L_R = T\sqrt{gh}(2m-1)/4$, where L_R is resonance length, T is tidal period, g is gravitational acceleration, and m is an integer. Channels close to the resonance length, as in Fig. 3(a–c), are most sensitive to length variations, and tidal ranges are amplified by 15–20% per meter of SLR. For all estuaries, SLR moves the system closer to a resonance state. It is worth mentioning that previous studies (Du et al., 2018; Hottinger, 2019; Khojasteh et al., 2019; Talke and Jay, 2020) showed that the tidal range in estuaries close to resonance is also sensitive to a change in water depth.

SLR may increase the water depth and the tidal prism, leading to a reduction in the frictional effect (Hoitink and Jay, 2016). This increase in tidal prism has implications for the stability of the entrance by actively changing the sediment transport and deposition dynamics in this zone (Duong et al., 2016, 2018). Variations in the normalized tidal prism under three SLR scenarios are presented in Fig. 4. From these results, it is apparent that tidal prism increases by up to 15% per meter of SLR. The reduced friction under SLR (increasing h) shifts the location of nodal points (i.e. points in a system where tidal amplitude is zero), as they occur at $(2m-1)L/4$ from the head of estuary, where m is an integer, and L is the wavelength (Du et al., 2018). Under SLR, these nodal points will be shifted in a downstream direction towards the entrance (Figs. 2 and 3). This phenomenon was previously observed in the main stem of the Chesapeake Bay estuary as reported by Du et al. (2018).

The phase difference (lag) between water surface elevation and tidal current velocity can be used as a proxy to identify tidal reflection along the estuary, as indicated in Fig. 5. The phase lags of 0° and 90° correspond to progressive (maximum energy propagation) and standing (zero

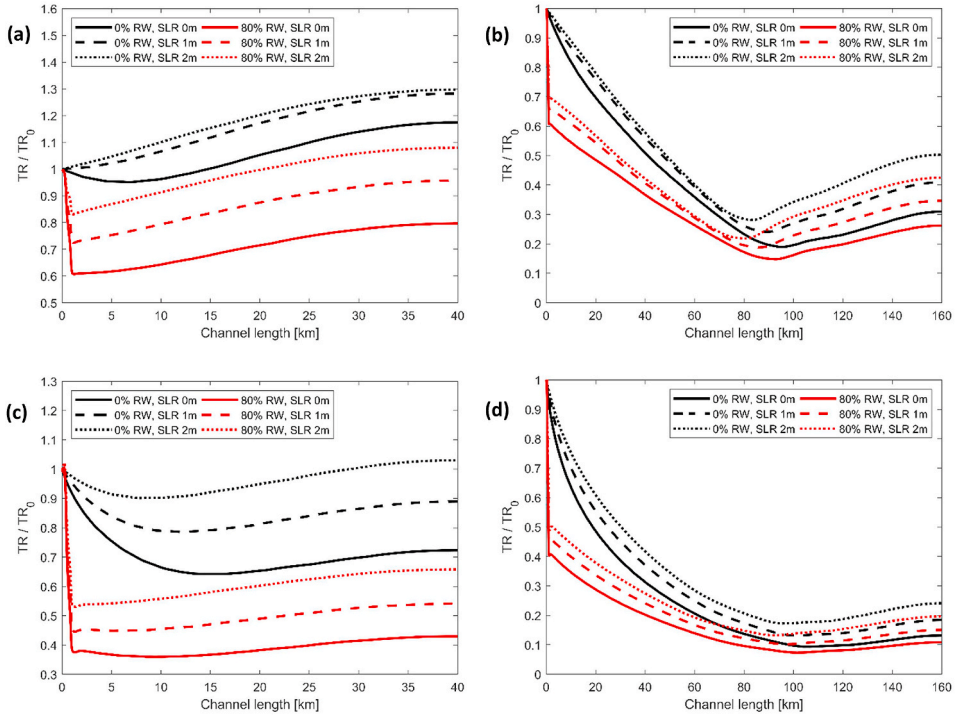

Fig. 2. The evolution of normalized tidal range in unrestricted and restricted estuaries of different lengths under SLR when: (a), (b) $TR_0 = 1$ m; (c), (d) $TR_0 = 4$ m.

energy propagation) waves, respectively (Lee et al., 2017). Mixed waves have phase lags between these two values. In all cases, tidal waves eventually become standing at the upstream ends due to tidal reflection induced by the closed end at the head. This phenomenon is more evident in short channels (Fig. 5(a, c)), where waves are close to standing throughout the majority of the channels. This is in line with the findings of Friedrichs (2010) who demonstrated that the phase lag in short and shallow estuaries is almost 90°. The longer the channel is, the less energy is available for the tidal waves to undergo reflection when reaching the head of the estuary due to the frictional losses (Fig. 5(b, d)). However, tidal reflection still presents weakly at the upper end of the long channels, confirming the findings of van Rijn (2011) who stated that reflection in closed end channels is significant in 1/3 of the most landward part. Further, SLR and entrance restriction impact the phase difference. These two factors generally move the mixed tidal waves towards more standing waves, producing tidal amplification. This was also observed in real-world estuaries such as the Chesapeake Bay and Delaware Bay in which SLR increased the phase lag in these two estuarine systems, generating standing waves and tidal amplification due to reflection at the upper ends (Lee et al., 2017).

3.2. Changes in tidal current velocity

This variation in tidal current velocity associated with a change in estuarine depth due to SLR impacts the energy dissipation in the estuarine system. Fig. 6 shows how SLR, entrance condition, channel length, and tidal forcing influence tidal current velocity. As expected, a higher tidal range at the mouth results in a higher flow velocity due to its higher energy. Further, the maximum tidal current velocity is higher inside the restriction zone of restricted channels but is then lower into the estuary part compared to unrestricted channels. These findings are reflected in real cases such as in Tauranga Harbour, a barrier-enclosed lagoon in New Zealand with restricted entrance, where current velocity reduced from 0.8 m/s at the entrance to 0.25 m/s in the upstream section (de Ruiter et al., 2017).

SLR has a negligible effect on the maximum tidal current velocity observed along different closed end estuaries. Even for open end estuaries (without reflection), van Rijn (2011) showed that the maximum current velocities for three depths of 5, 10, and 15 m are almost identical. However, the distributions of flood velocity (incoming tide) and ebb velocity (outgoing tide) are impacted by SLR for all channels tested. Fig. 7 illustrates the maximum flood/ebb velocity distributions in the form of probability density functions (PDFs), highlighting the likelihood of occurrence of any ebb/flood velocity value. It can be seen that SLR slightly modifies the maximum ebb velocities (Fig. 7(a, b)), and the maximum flood velocities (Fig. 7(c, d)) in both restricted and unrestricted estuaries. These distributions are changed, with higher velocities found when the mean sea level increases. This finding is highlighted by Tang et al. (2014) who found that SLR tends to increase the flow velocity in estuaries located at the coast of New Jersey, USA, leading to an increase in average marine hydrokinetic energy ($\propto U^3$) by up to 43% per meter of SLR. Any alterations in velocity distribution may cause changes to the estuarine morphology via altered sediment dynamics which in turn alter the estuarine hydrodynamics (de Jonge et al., 2014), with implications to estuarine turbidity, harbour siltation, ecological protection, and biogeochemical cycling (Yu et al., 2014).

3.3. Changes in tidal asymmetry

Tidal asymmetry is a phenomenon of tidal wave deformation that results in an unequal duration of the rise and fall of the tidal amplitude and offsets between the strength of the flood and ebb velocities (Dronkers, 1986; Guo et al., 2019). Tidal asymmetry creates unique patterns of sediment transport and deposition within an estuary and hence, represents a key driver of estuarine morphodynamics (Swart and Zimmerman, 2009). An estuary is flood dominated if the falling tide is longer than the rising tide (called tidal duration asymmetry), or the maximum flood currents are stronger than ebb currents (called peak current asymmetry) (Guo et al., 2019). These patterns are the opposite in an ebb dominated estuary. Flood dominated systems typically experience sediment ingress and basin infilling, while ebb dominated systems experience sediment flushing (export) and tidal emptying (Aubrey and Speer, 1985; Passeri et al., 2015c). Several harmonic and statistical

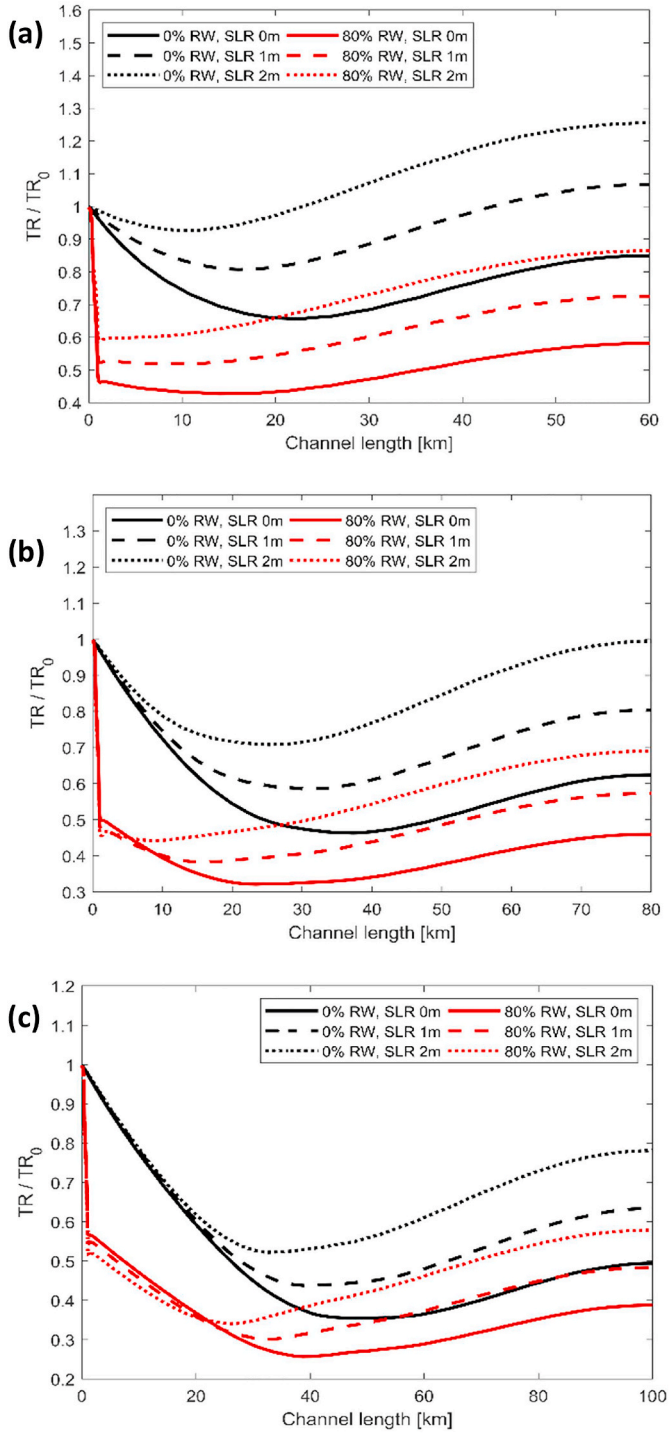

Fig. 3. The evolution of normalized tidal range in unrestricted and restricted estuaries under SLR when $TR_0 = 1$ m for (a) $Z = 60$ km; (b) $Z = 80$ km; (c) $Z = 100$ km.

methods have been introduced by Guo et al. (2019) to measure tidal asymmetry by calculating the PDF of tidal heights and tidal durations. Here, two statistical methods, skewness coefficient (by measuring tidal heights) and transformed skewness coefficient (by measuring tidal durations), are adopted from Guo et al. (2019) to quantify the degree of asymmetry in the simulated cases. A positive value of skewness denotes a stronger maximum flood current than ebb current, resulting in flood domination. The converse is valid for an ebb dominated system. For transformed skewness, a positive value implies longer rising tidal durations than falling tide durations and leads to an ebb dominated system, while a positive value indicates a flood dominated system.

The changes in tidal asymmetry of various estuaries are shown in Fig. 8, by analysing the skewness coefficient. Analyses on the transformed skewness coefficient are available in Fig. S2 in the Supplementary Material. Estuaries of 40 and 160 km are flood dominated throughout the majority of the channels with a sharp increase in flood domination after the restricted entrance. The flood domination tends to increase from the entrance towards the head of the estuary, intensifying sediment import mechanisms (van Maren et al., 2015; Winterwerp, 2011). The observed flood domination is consistent with previous theoretical findings of Friedrichs and Madsen (1992) and Friedrichs (2010) where they defined asymmetry as $\gamma = a/ < h > - 0.5\Delta B/ < B >$. Here, a is tidal amplitude, $< >$ indicates absolute values, B is channel width, and ΔB is the amplitude of the temporal channel width variation. A positive value of γ denotes a flood dominated system and a negative value presents an ebb dominated system. In hard coastlines with no overland flooding, the term $\Delta B/ < B >$ is zero, indicating that asymmetry is always positive theoretically. The increased flood domination at the estuarine head can be justified by a constant energy loss from the M_2 tidal component due to friction, which is then partially transferred to higher frequencies (overtides), leading to a pronounced flood domination (Blanton et al., 2002).

Additionally, SLR tends to decrease the flood domination in the system by decreasing the friction. Ebb domination is observable in estuaries with extensive floodplains, tidal flats, and weak friction (Speer and Aubrey, 1985). However, the assumed vertical walls around the edges of simulated models prevent flooding of adjacent low-lying lands under SLR. Therefore, the only consequence of SLR considered here is lower friction due to increasing depth that diminishes the flood domination. This is also explainable by checking γ, as the effect of tidal flats or floodplains can be included in term $\Delta B/ < B >$, whereas this term is always zero when no overland flooding occurs. To illustrate in real sites, the Keum River estuary in Korea is flood dominated as the estuary is shallow, leading to a strong energy dissipation in the estuarine system from bed friction (Kang and Jun 2003). Whereas, the Youngsan River estuary in Korea is ebb dominated due to the presence of vast tidal flats (Kang and Jun 2003).

3.4. Application of clustering and data analysis in estuarine hydrodynamics

Based on the clustering and data analysis techniques (see Supplementary Material), tidal forcing at the estuary mouth was found to be the key factor that controls the hydrodynamics, followed by estuarine length. Therefore, all investigated estuaries were classified into four groups as (1) $Z = 40$ km, $TR_0 = 1$ m; (2) $Z = 160$ km, $TR_0 = 1$ m; (3) $Z = 40$ km, $TR_0 = 4$ m; and (4) $Z = 160$ km, $TR_0 = 4$ m. Fig. 9 shows the Pearson Correlation matrices, highlighting the linear correlation between the variables within these four groups. This correlation ranged from -1 to 1, with -1 indicating a perfect negative linear correlation, 0 denoting no linear correlation, and 1 presenting a perfect positive linear correlation. It can be seen that, for example, SLR has an insignificant effect on the maximum tidal current velocity in all groups, highlighted by the correlation coefficients close to 0. However, the normalized tidal range along the different estuaries is expected to increase under SLR. The magnitude of this increase depends on the channel length. To illustrate, when $TR_0 = 1$ m, the Pearson correlation factors are 0.44 and 0.76 for $Z = 40$ km and $Z = 160$ km, respectively. The skewness coefficient decreases under SLR, indicating a reduction in flood domination in the system (also indicated in Fig. 8). A reverse trend is observable for the transformed skewness coefficient. Further, the narrower inlets increase the maximum current velocities (a positive correlation factor) and decrease the normalized tidal range, particularly in shorter channels (a negative correlation factor). Although the correlations between estuarine variables are often nonlinear, the Pearson

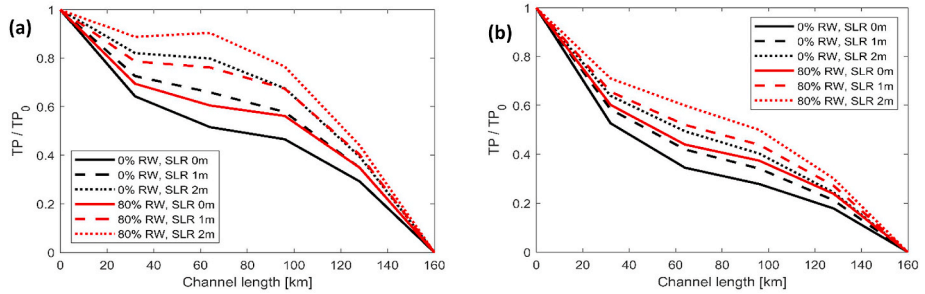

Fig. 4. The evolution of normalized tidal prism in an unrestricted and restricted 160 km estuary under SLR when: (a) $TR_0 = 1$ m; (b) $TR_0 = 4$ m.

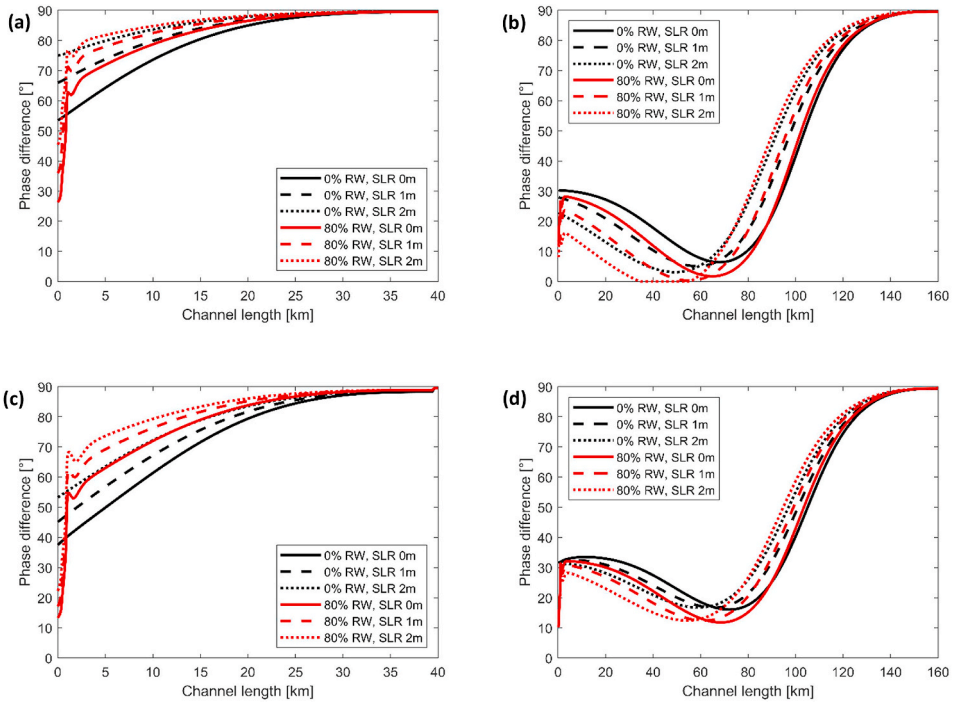

Fig. 5. Tidal phase variations in unrestricted and restricted 40 km and 160 km channels under SLR when: (a), (b) $TR_0 = 1$ m; (c), (d) $TR_0 = 4$ m.

correlation provides a reasonable and robust first pass estimate of empirical relationships between estuarine parameters (Fig. 9). More advanced techniques (e.g. maximal information coefficient) are available to determine the nonlinear correlations between variables in large datasets (e.g. Reshef et al. (2011)), but these have not been employed here.

4. Discussion

4.1. Entrance restriction: A solution to offset SLR induced tidal range amplification?

As demonstrated in the estuary types examined in this study, an increase in mean sea level increases the estuarine tidal prism and reduces the bed friction, indicating that estuarine tidal range can be amplified under SLR. This means that maximum water levels inside estuaries could rise significantly more than just by the increase in mean sea level at the ocean boundary. Increased development around estuaries is typically accompanied by the construction of seawalls and dykes as well as land reclamation and this process has disconnected the intertidal areas that used to add storage space and friction to estuarine systems and thereby naturally limit the flood risk (De Vriend et al., 2011; Leuven et al., 2019).

Among the factors influencing estuarine hydrodynamics under SLR, entrance structure can be dredged or restricted to regulate the tides flowing in and out of the estuary, protecting people and assets against increasing flooding under SLR or assisting with navigation by maintaining an efficient flow through the estuarine system. As such, the engineered restriction of entrances could be considered as a potential solution to mitigate SLR induced tidal range amplification in prismatic estuaries.

Fig. 10 shows the initial tidal range attenuation (i.e. tidal range 1 km away from the entrance) for different levels of entrance restriction in a channel of 160 km. It is obvious that the tidal range decreases exponentially as *RW*% increases (Fig. 10(a, c)), and only minor tidal range reduction occurs when the entrance is restricted by less than 40%. Tidal range dampening is more evident as the tidal range at the mouth increases. Fig. 10(b, d) highlights that $RW = 50$–70% is potentially sufficient to fully offset the tidal range amplification caused by SLR. In practical terms, a restricted entrance can be established as a fixated and elevated entrance berm or a series of tidal gates across the entrance channel that both help limiting tidal flow and exchange. Importantly, however, permanently restricting an entrance would not only lead to reduced daily tidal flushing, but also to reduced and delayed drainage of the estuary during and after river-driven floods. In addition, such an intervention could disturb the geomorphological equilibrium of an

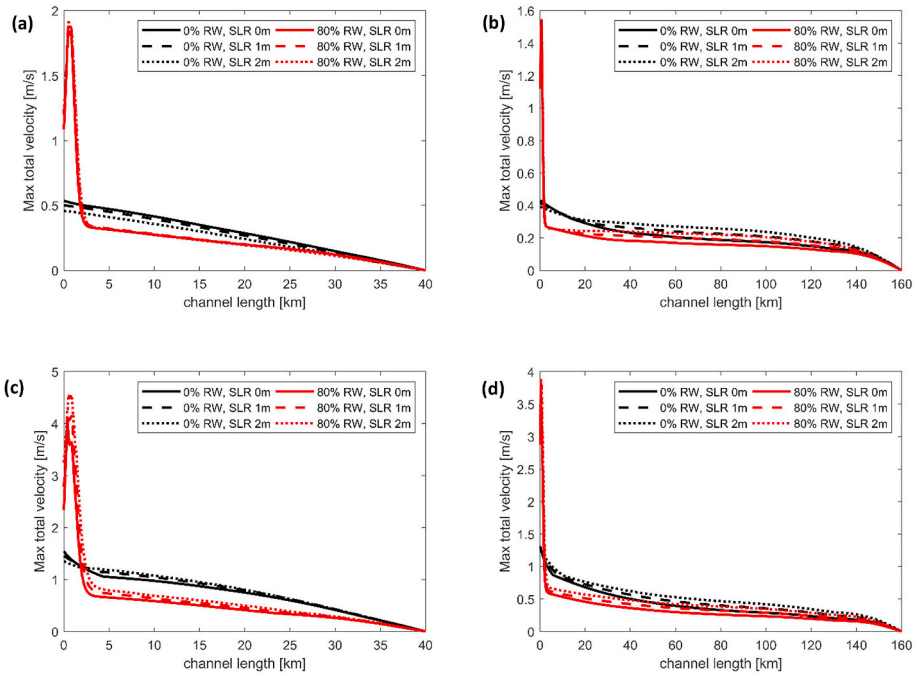

Fig. 6. Maximum tidal current velocity variations in unrestricted and restricted channels of varying lengths under SLR when: (a), (b) $TR_0 = 1$ m; (c), (d) $TR_0 = 4$ m.

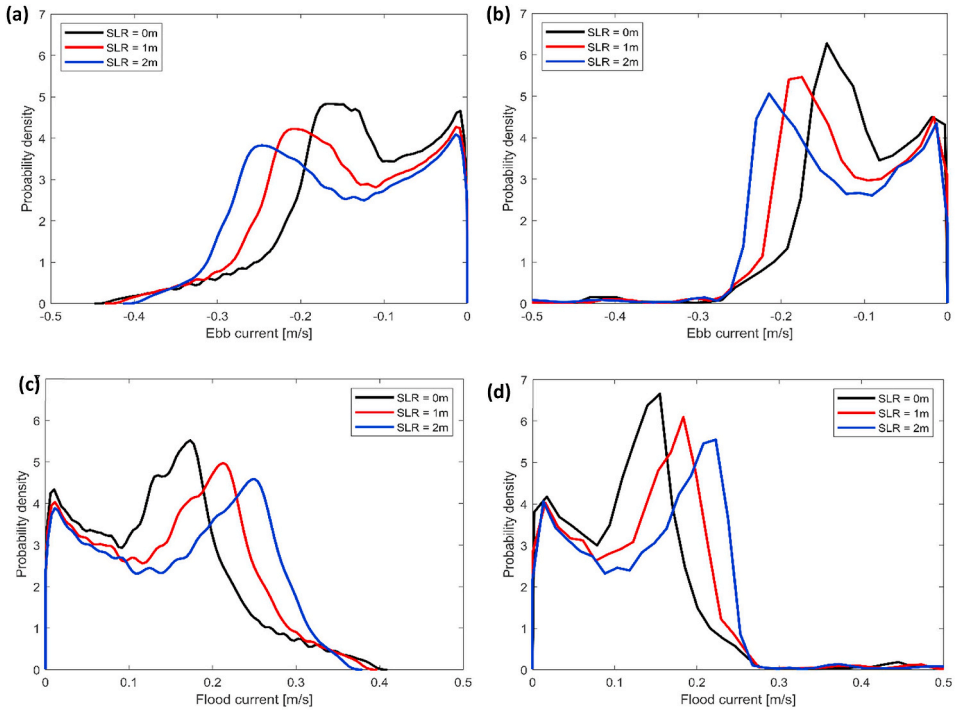

Fig. 7. Probability density distributions of ebb and flood velocities in a channel of 160 km under SLR when $TR_0 = 1$ m for: (a), (c) unrestricted channels; (b), (d) *RW* = 80% restricted channels.

estuary entrance, which can lead to a significant redistribution of sediment in and around the entrance via bank and channel erosion and accretion. All these complexities need to be carefully assessed before making any related management decision.

4.2. Idealised approach: potentials, limitations, and recommendations

The hydrodynamic responses of estuaries to SLR are highly individualistic, depending on the driving forces as well as estuarine geometry, bathymetry, friction, and availability of intertidal areas. Further, running a well-calibrated hydrodynamic model for every single estuary worldwide is still challenging as sufficient resources are often not available (e.g. due to lack of high-quality field data). To date, a systematic study to indicate how SLR is changing estuarine tidal dynamics in estuaries with significantly restricted entrances is absent in the literature. This gap was partially covered in this study by using a large ensemble of idealised estuary models of varying scale and degree of entrance restriction. Throughout this paper, it was highlighted that the

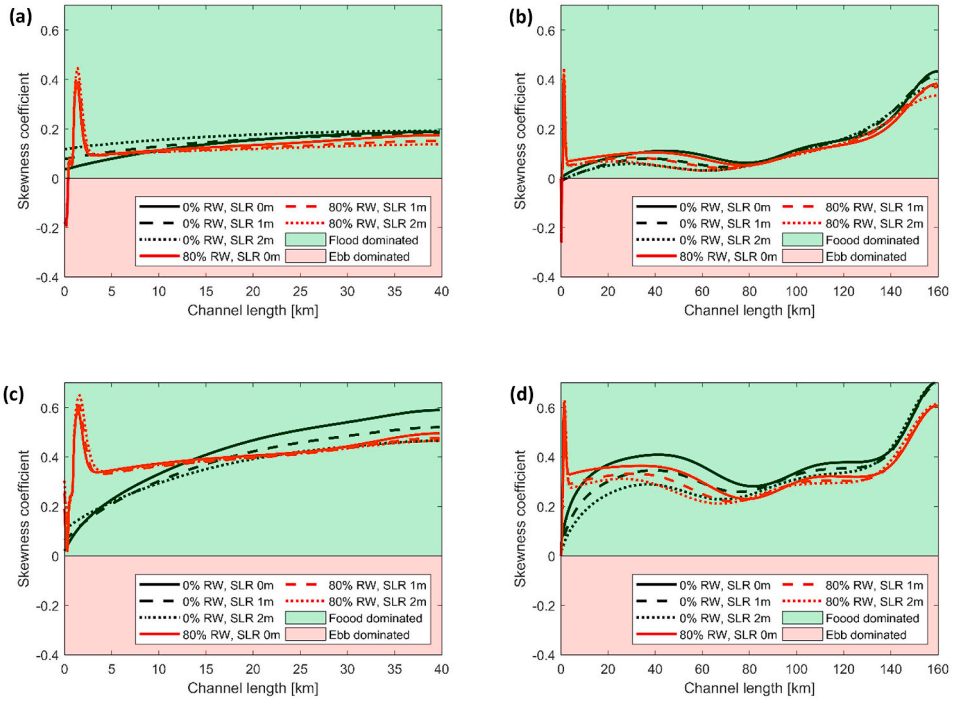

Fig. 8. Skewness coefficient variations in unrestricted and restricted channels under SLR when: (a), (b) $TR_0 = 1$ m; (c), (d) $TR_0 = 4$ m.

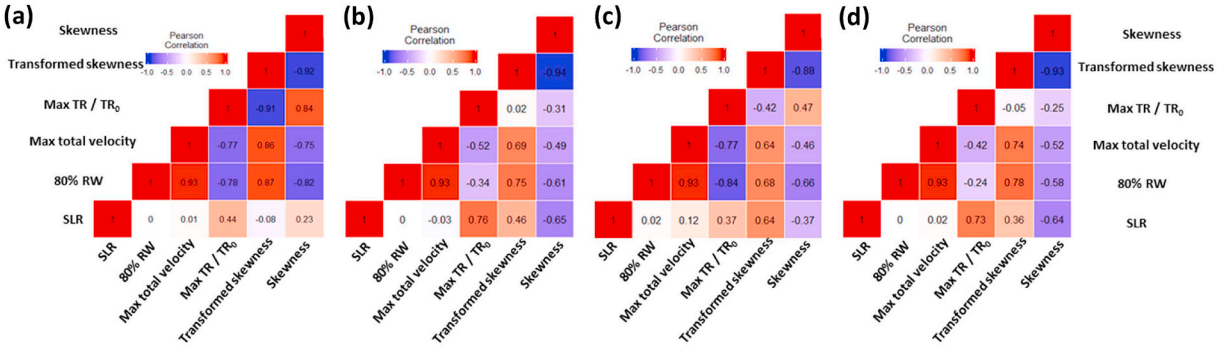

Fig. 9. Pearson correlation matrices for: (a) $Z = 40$ km, $TR_0 = 1$ m; (b) $Z = 160$ km, $TR_0 = 1$ m; (c) $Z = 40$ km, $TR_0 = 4$ m; and (d) $Z = 160$ km, $TR_0 = 4$ m.

findings from the idealised approach are in good agreement with the analytical/theoretical solutions and hydrodynamic assessments of some real-world estuaries. As such, this methodology, despite having certain limitations, allows a theoretical assessment of any given idealised estuary. The learnings provided by idealised cases can be transferred back to a particular range of real-world estuarine conditions, based on their dominant physical characteristics (see Du et al. (2018) and Talke and Jay (2020)).

While most previous studies have focused only on predicting the future high tide levels and associated inundation due to SLR, the present study illustrates that to carefully examine the altered energy dynamics within estuaries, changes to tidal range (both low and high tides), tidal prism, tidal phase, tidal current velocity, tidal asymmetry, tidal reflection (or resonance), location of nodal points, and friction under SLR should be taken into consideration. To illustrate, a higher low tide level under SLR brings about reduced drainage and prolonged inundation of low-lying lands, and a higher high tide increases nuisance (sunny day) or destructive flood events. The changes in low and high tides under SLR (Fig. S3 in the Supplementary Material) demonstrate that SLR generally increases the tidal range within prismatic estuaries through modification of both low and high tides. The variations in low and high tide levels can also impact estuarine navigation. While an increased mean sea level may permit deeper-drafted vessels into the estuary, the increased occurrence of higher tidal current velocities under SLR may provide less flexibility for management of ports, harbours, and estuaries (Meyers and Luther, 2020).

SLR may induce higher medium current velocities and shift the overall tidal asymmetry towards a weaker flood dominated system, resulting in increased transport of sediments out of the estuary (flushing) and vulnerability of coastal wetlands to SLR, as accretion depends on the amount of sediment available in the system. The change in sediment accretion/deposition dynamics will likely alter the geomorphology of the estuarine system, which has implications with regards to further changes in tidal dynamics through a feedback loop. Changes in estuarine hydrodynamics also influence tidal power, mixing, circulation, and saltwater intrusion (Chua and Xu, 2014; Tang et al., 2014).

If a major river discharge exists in the upstream reaches, tidal energy can be further dissipated, counterbalancing the tidal amplification due to reflection at the head. For the estuaries tested here, estuaries are assumed to be tidally dominated, indicating that no/minor river discharge is present. The increased mean sea level under SLR can act as an elevated platform for waves and storm surges (in addition to tides) that can further increase the complexity of predicting estuarine

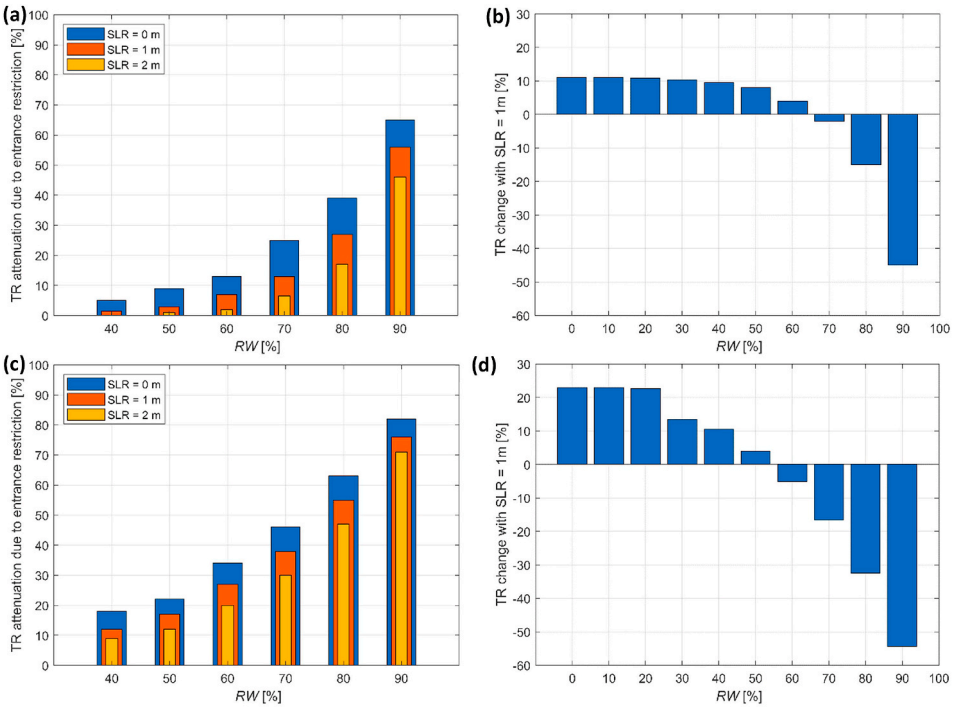

Fig. 10. Tidal range variations close to estuarine mouth when $Z = 160$ km for various RW% when: (a) SLR = 0, 1, 2 m and $TR_0 = 1$ m; (b) SLR = 1 m and $TR_0 = 1$ m; (c) SLR = 0, 1, 2 m and $TR_0 = 4$ m; (d) SLR = 1 m and $TR_0 = 4$ m.

hydrodynamics (Moftakhari et al., 2017; Oppenheimer et al., 2019). Nevertheless, for future studies it is recommended to consider a range of river inflows, wave and wind driving forces and storm surges.

It is also proposed to test various depths and frictions (e.g. Manning coefficient) to examine how they may influence hydrodynamics of different estuaries as this study only considered a single value for these parameters. Here, tide is driven by a pure M_2 tide, but it is recommended to consider other relevant semidiurnal and diurnal tidal constituents. The flood walls assumed at the edges of the modelled channels are realistic where extensive protective walls are implemented at present-day coastlines, inducing tidal amplification and flood domination. However, there are estuaries worldwide that are surrounded by large tracts of wetlands and tidal flats without being anthropogenically protected. The responses of these types of estuaries to SLR should be then compared with those reported here.

5. Conclusions

Due to the proximity of the open ocean and the low-lying nature of estuaries, hundreds of millions of people who live near these systems are susceptible to SLR. The majority of previous efforts to characterize estuarine responses to SLR have either used static approaches that fail to consider the full tidal wave dynamics, or have focused on a few selected real-world case studies, which provide outcomes that are linked to a specific site. To partially address this limitation, this study used an idealised hydrodynamic framework to assess the likely impacts of SLR on tidal responses of prismatic estuaries of varying length, width, and entrance restrictions. By using an ensemble of idealised estuarine models, as well as clustering and data analysis techniques, the key driving mechanisms and responses were highlighted by analysing the changes in tidal range, tidal prism, phase lag, tidal current velocity, tidal asymmetry, location of nodal points, and reflection (resonance) under SLR. Future work could expand our systematic approach to also incorporate converging estuaries, river inflows, varying friction, and bed slope. The key findings of the present study are summarized in Table 2. The following conclusions can be drawn:

- Tidal forcing, estuarine length, and entrance restriction control the tidal dynamics of prismatic estuaries under SLR. SLR increases the mean sea level, leading to reduced friction, increased wave celerity and wavelength, as well as moving the location of nodal points in a seaward direction.
- SLR generally increases the tidal range within prismatic estuaries by modifying both low and high tide levels. Therefore, the inundation extent will be greater than what would be expected by simply adjusting existing water levels upwards. Under SLR, short estuaries

Table 2
Changes in parameters of prismatic estuaries with restricted and unrestricted entrances under SLR.

Estuarine parameter	Location	Unrestricted		Highly restricted	
		Short estuary	Long estuary	Short estuary	Long estuary
Tidal range	Entrance	Increasing	Increasing	Increasing	Increasing
	Estuary	Increasing	Increasing	Increasing	Increasing
Tidal phase lag	Entrance	Increasing	Decreasing	Increasing	Decreasing
	Estuary	Increasing	Decreasing-Increasing	Increasing	Decreasing-Increasing
Maximum flow velocity	Entrance	Decreasing	Unchanged	Increasing	Unchanged
	Estuary	Unchanged	Unchanged	Unchanged	Increasing
Flood domination	Entrance	Increasing	Decreasing	Unchanged	Unchanged
	Estuary	Depends on tidal forcing	Decreasing	Unchanged	Decreasing

experience amplified tidal range and standing waves due to reflection at the head, long estuaries experience attenuated tidal range and mixed waves due to bed friction, and a mixed response is observable in estuaries close to resonance. Restricting the cross-section of the entrance significantly reduces the tidal range but its influence on the phase lag is negligible.

- SLR has negligible impact on the maximum tidal current velocity but changes the distribution of mean current velocities, with higher velocities found when the mean sea level increases. All tested channels were initially flood dominated, and this domination tends to increase towards the head due to reflection and decreases under SLR due to weakened friction. In estuaries with restricted entrances, maximum flow velocity is higher in the restricted part of the estuary but is then lower in the upstream part compared to unrestricted estuaries.
- Finally, the concept of restricting the estuarine entrance can be introduced as a potential solution to counterbalance SLR induced tidal amplification. However, it is important to consider the associated effects on entrance stability, navigation, flooding, and safety of swimmers before making any management decision.

CRediT authorship contribution statement

Danial Khojasteh: Conceptualization, Methodology, Formal analysis, Writing - original draft, Writing - review & editing. **Steve Hottinger:** Methodology, Formal analysis, Writing - original draft. **Stefan Felder:** Conceptualization, Writing - review & editing, Supervision. **Giovanni De Cesare:** Writing - review & editing, Supervision. **Valentin Heimhuber:** Conceptualization, Writing - review & editing. **David J. Hanslow:** Writing - review & editing. **William Glamore:** Conceptualization, Writing - review & editing, Supervision.

Declaration of competing interest

The authors declare that they have no known competing financial interests or personal relationships that could have appeared to influence the work reported in this paper.

Acknowledgments

The authors thank Professor Ian King for helpful discussions regarding RMA-2 functions. Danial Khojasteh is supported by a UNSW Scientia PhD Scholarship.

Appendix A. Supplementary data

Supplementary data to this article can be found online at https://doi.org/10.1016/j.ecss.2020.106941.

References

Anderson, T.R., Fletcher, C.H., Barbee, M.M., Romine, B.M., Lemmo, S., Delevaux, J.M. S., 2018. Modeling multiple sea level rise stresses reveals up to twice the land at risk compared to strictly passive flooding methods. Sci. Rep. 8, 14484.

Arcement, G.J., Schneider, V.R., 1989. Guide for Selecting Manning's Roughness Coefficients for Natural Channels and Flood Plains. US Government Printing Office, Washington, DC, United States.

Aretxabaleta, A.L., Ganju, N.K., Butman, B., Signell, R.P., 2017. Observations and a linear model of water level in an interconnected inlet-bay system. J. Geophys. Res.: Oceans 122, 2760–2780.

Aubrey, D.G., Speer, P.E., 1985. A study of non-linear tidal propagation in shallow inlet/estuarine systems Part I: observations. Estuarine. Coastal and Shelf Science 21, 185–205.

Bamber, J.L., Oppenheimer, M., Kopp, R.E., Aspinall, W.P., Cooke, R.M., 2019. Ice sheet contributions to future sea-level rise from structured expert judgment. Proc. Natl. Acad. Sci. Unit. States Am. 116, 11195–11200.

Bergillos, R.J., Rodriguez-Delgado, C., Iglesias, G., 2019. Wave farm impacts on coastal flooding under sea-level rise: a case study in southern Spain. Sci. Total Environ. 653, 1522–1531.

Blanton, J.O., Lin, G., Elston, S.A., 2002. Tidal current asymmetry in shallow estuaries and tidal creeks. Continent. Shelf Res. 22, 1731–1743.

Bruun, P., Gerritsen, F., 1960. Stability of coastal inlets. Coastal Engineering Proceedings 1 (7), 23.

Callaghan, D.P., Wainwright, D.J., Hanslow, D.J., 2020. Consideration of uncertainty in sea level rise in Australia's most exposed estuary: a discussion on allowances under different epistemic uncertainties. Coast. Eng. 159, 103718.

Cerralbo, P., Grifoll, M., Valle-Levinson, A., Espino, M., 2014. Tidal transformation and resonance in a short, microtidal Mediterranean estuary (Alfacs Bay in Ebre delta). Estuarine. Coastal and Shelf Science 145, 57–68.

Chen, K., McAneney, J., 2006. High-resolution estimates of Australia's coastal population. Geophys. Res. Lett. 33.

Chua, V.P., Xu, M., 2014. Impacts of sea-level rise on estuarine circulation: an idealized estuary and San Francisco Bay. J. Mar. Syst. 139, 58–67.

de Jonge, V.N., Schuttelaars, H.M., van Beusekom, J.E.E., Talke, S.A., de Swart, H.E., 2014. The influence of channel deepening on estuarine turbidity levels and dynamics, as exemplified by the Ems estuary. Estuar. Coast Shelf Sci. 139, 46–59.

de Ruiter, P.J., Mullarney, J.C., Bryan, K.R., Winter, C., 2017. The influence of entrance constriction on hydrodynamics and intertidal morphology within estuarine basins. Australasian Coasts & Ports 2017: Working with Nature 378.

De Vriend, H.J., Wang, Z.B., Ysebaert, T., Herman, P.M.J., Ding, P., 2011. Eco-morphological problems in the yangtze estuary and the western scheldt. Wetlands 31, 1033–1042.

DeConto, R.M., Pollard, D., 2016. Contribution of Antarctica to past and future sea-level rise. Nature 531, 591–597.

Dronkers, J., 1986. Tidal asymmetry and estuarine morphology. Neth. J. Sea Res. 20, 117–131.

Du, J., Shen, J., Zhang, Y.J., Ye, F., Liu, Z., Wang, Z., Wang, Y.P., Yu, X., Sisson, M., Wang, H.V., 2018. Tidal response to sea-level rise in different types of estuaries: the importance of length, bathymetry, and geometry. Geophys. Res. Lett. 45, 227–235.

Duong, T.M., Ranasinghe, R., Thatcher, M., Mahanama, S., Wang, Z.B., Dissanayake, P. K., Hemer, M., Luijendijk, A., Bamunawala, J., Roelvink, D., Walstra, D., 2018. Assessing climate change impacts on the stability of small tidal inlets: Part 2 - data rich environments. Mar. Geol. 395, 65–81.

Duong, T.M., Ranasinghe, R., Walstra, D., Roelvink, D., 2016. Assessing climate change impacts on the stability of small tidal inlet systems: why and how? Earth Sci. Rev. 154, 369–380.

Elmoustafa, A.M., 2017. Evaluation of water intake location suitability using a hydrodynamic approach. Journal of Applied Water Engineering and Research 5, 31–39.

Fairbridge, R.W., 1980. Encyclopedia of Geomorphology, New York.

FitzGerald, D., Buynevich, I., Davis Jr., R., Fenster, M., 2002. New England tidal inlets with special reference to riverine-associated inlet systems. Geomorphology 48, 179–208.

Friedrichs, C.T., 2010. Barotropic tides in channelized estuaries. Contemporary issues in estuarine physics 27–61.

Friedrichs, C.T., Madsen, O.S., 1992. Nonlinear diffusion of the tidal signal in frictionally dominated embayments. J. Geophys. Res.: Oceans 97, 5637–5650.

Grenfell, S.E., Callaway, R.M., Grenfell, M.C., Bertelli, C.M., Mendzil, A.F., Tew, I., 2016. Will a rising sea sink some estuarine wetland ecosystems? Sci. Total Environ. 554–555, 276–292.

Guo, L., Wang, Z.B., Townend, I., He, Q., 2019. Quantification of tidal asymmetry and its nonstationary variations. J. Geophys. Res.: Oceans 124, 773–787.

Guo, W., Wang, X.H., Ding, P., Ge, J., Song, D., 2018. A system shift in tidal choking due to the construction of Yangshan Harbour, Shanghai, China. Estuarine. Coastal and Shelf Science 206, 49–60.

Hanslow, D.J., Morris, B.D., Foulsham, E., Kinsela, M.A., 2018. A regional scale Approach to assessing current and potential future exposure to tidal inundation in different types of estuaries. Sci. Rep. 8, 7065.

Hinwood, J., Aoki, S.-I., Okabe, T., 2017. Effect of regulation of the inlet channel on tides and water levels in Lake Hamana, Japan. Coast Eng. J. 59, 1750016.

Hinwood, J.B., McLean, E.J., 2015. Predicting the dynamics of intermittently closed/open estuaries using attractors. Coast. Eng. 99, 64–72.

Hinwood, J.B., McLean, E.J., 2018. Tidal inlets and estuaries: comparison of Bruun, escoffier, O'Brien and attractors. Coast. Eng. 133, 92–105.

Hinwood, J.B., McLean, E.J., Wilson, B.C., 2012. Non-linear dynamics and attractors for the entrance state of a tidal estuary. Coast. Eng. 61, 20–26.

Hoeke, R.K., McInnes, K.L., Kruger, J.C., McNaught, R.J., Hunter, J.R., Smithers, S.G., 2013. Widespread inundation of Pacific islands triggered by distant-source wind-waves. Global Planet. Change 108, 128–138.

Hoitink, A.J.F., Jay, D.A., 2016. Tidal river dynamics: implications for deltas. Rev. Geophys. 54, 240–272.

Horton, B.P., Khan, N.S., Cahill, N., Lee, J.S.H., Shaw, T.A., Garner, A.J., Kemp, A.C., Engelhart, S.E., Rahmstorf, S., 2020. Estimating global mean sea-level rise and its uncertainties by 2100 and 2300 from an expert survey. npj Climate and Atmospheric Science 3, 18.

Hottinger, S., 2019. Effects of Entrance Conditions on Tidal Hydrodynamics in Idealized Prismatic Estuaries under Sea Level Rise, Master Thesis. École Polytechnique Fédérale de Lausanne, Lausanne, Switzerland.

Kang, J.W., Jun, K.S., 2003. Flood and ebb dominance in estuaries in Korea. Estuar. Coast Shelf Sci. 56, 187–196.

Khojasteh, D., Glamore, W., Heimhuber, V., Hottinger, S., Felder, S., 2019. Implications of Tidal Resonance and Water Depth on Predicting Sea Level Rise in Estuaries. Australasia Coasts & Ports, Hobart, Australia.

Khojasteh, D., Tavakoli, S., Dashtimanesh, A., Dolatshah, A., Huang, L., Glamore, W., Sadat-Noori, M., Iglesias, G., 2020. Numerical analysis of shipping water impacting a step structure. Ocean Eng. 209, 107517.

King, I., 2013. A Two-Dimensional Finite Element Model for Flow in Estuaries and Streams. RMA-2, Users Guide, Version 8.4 T.
King, I., Donnell, B., Letter, J., McAnally, W., Thomas, W., 1997. Users Guide to RMA2 WES Version 4.5. The US Army Corps of Engineers–Waterways experiment laboratory, p. 240.
King, I.P., Norton, W., 1978. Recent application of RMA's finite element models for two-dimensional hydrodynamics and water quality. Proc. 2nd Int. Conf. on Finite Elements in Water Resources, London 281–299.
Kulp, S.A., Strauss, B.H., 2019. New elevation data triple estimates of global vulnerability to sea-level rise and coastal flooding. Nat. Commun. 10, 4844.
Kumbier, K., Carvalho, R.C., Woodroffe, C.D., 2018. Modelling hydrodynamic impacts of sea-level rise on wave-dominated Australian estuaries with differing geomorphology. J. Mar. Sci. Eng. 6, 66.
Le Souëf, K.E., Allen, S.E., 2014. Physical modeling of tidal resonance in a submarine canyon. J. Geophys. Res.: Oceans 119, 1324–1343.
Lee, S.B., Li, M., Zhang, F., 2017. Impact of sea level rise on tidal range in Chesapeake and Delaware Bays. J. Geophys. Res.: Oceans 122, 3917–3938.
Leuven, J.R.F.W., Pierik, H.J., Vegt, M.v.d., Bouma, T.J., Kleinhans, M.G., 2019. Sea-level-rise-induced threats depend on the size of tide-influenced estuaries worldwide. Nat. Clim. Change 9, 986–992.
MacMahan, J., van de Kreeke, J., Reniers, A., Elgar, S., Raubenheimer, B., Thornton, E., Weltmer, M., Rynne, P., Brown, J., 2014. Fortnightly tides and subtidal motions in a choked inlet. Estuarine. Coastal and Shelf Science 150, 325–331.
McSweeney, S.L., Kennedy, D.M., Rutherfurd, I.D., Stout, J.C., 2017. Intermittently closed/open Lakes and lagoons: their global distribution and boundary conditions. Geomorphology 292, 142–152.
Melet, A., Meyssignac, B., Almar, R., Le Cozannet, G., 2018. Under-estimated wave contribution to coastal sea-level rise. Nat. Clim. Change 8, 234–239.
Meyers, S.D., Luther, M.E., 2020. The Impact of Sea Level Rise on Maritime Navigation within a Large, Channelized Estuary. Maritime Policy & Management, pp. 1–17.
Moftakhari, H., Schubert, J.E., AghaKouchak, A., Matthew, R.A., Sanders, B.F., 2019. Linking statistical and hydrodynamic modeling for compound flood hazard assessment in tidal channels and estuaries. Adv. Water Resour. 128, 28–38.
Moftakhari, H.R., Salvadori, G., AghaKouchak, A., Sanders, B.F., Matthew, R.A., 2017. Compounding effects of sea level rise and fluvial flooding. Proc. Natl. Acad. Sci. Unit. States Am. 114, 9785–9790.
Nielsen, A.F., Gordon, A.D., 2017. Long term impacts of jetties and training walls on estuarine hydraulics and ecologies. Coastal Wetlands: Alteration and Remediation. Springer, pp. 317–355.
NOAA, 2017. Method Description: Detailed Method for Mapping Sea Level Rise Inundation.
Oppenheimer, M., Glavovic, B., Hinkel, J., van de Wal, R., Magnan, A.K., Abd-Elgawad, A., Cai, R., Cifuentes-Jara, M., Deconto, R.M., Ghosh, T., Hay, J., Isla, F., Marzeion, B., Meyssignac, B., Sebesvari, Z., 2019. Sea Level Rise and Implications for Low Lying Islands, Coasts and Communities; IPCC Special Report on the Ocean and Cryosphere in a Changing Climate, IPCC Special Report on the Ocean and Cryosphere in a Changing Climate.
Palmer, K., Watson, C., Fischer, A., 2019. Non-linear interactions between sea-level rise, tides, and geomorphic change in the Tamar Estuary, Australia. Estuar. Coast Shelf Sci. 225, 106247.
Passeri, D.L., Hagen, S.C., Bilskie, M.V., Medeiros, S.C., 2015a. On the significance of incorporating shoreline changes for evaluating coastal hydrodynamics under sea level rise scenarios. Nat. Hazards 75, 1599–1617.
Passeri, D.L., Hagen, S.C., Medeiros, S.C., Bilskie, M.V., 2015b. Impacts of historic morphology and sea level rise on tidal hydrodynamics in a microtidal estuary (Grand Bay, Mississippi). Continent. Shelf Res. 111, 150–158.
Passeri, D.L., Hagen, S.C., Medeiros, S.C., Bilskie, M.V., Alizad, K., Wang, D., 2015c. The dynamic effects of sea level rise on low-gradient coastal landscapes: a review. Earth's Future 3, 159–181.
Prandle, D., 2003. Relationships between tidal dynamics and bathymetry in strongly convergent estuaries. J. Phys. Oceanogr. 33, 2738–2750.
Proudfoot, M., Valentine, E.M., Evans, K.G., King, I., 2018. Calibration of a marsh-porosity finite element model: case study from a macrotidal creek and floodplain in northern Australia. J. Hydraul. Eng. 144, 05017005.
Pye, K., Blott, S.J., 2014. The geomorphology of UK estuaries: the role of geological controls, antecedent conditions and human activities. Estuar. Coast Shelf Sci. 150, 196–214.
Rao, P., 2005. A parallel RMA2 model for simulating large-scale free surface flows. Environ. Model. Software 20, 47–53.
Reshef, D.N., Reshef, Y.A., Finucane, H.K., Grossman, S.R., McVean, G., Turnbaugh, P.J., Lander, E.S., Mitzenmacher, M., Sabeti, P.C., 2011. Detecting novel associations in large data sets. Science 334, 1518–1524.
Rodríguez, J.F., Saco, P.M., Sandi, S., Saintilan, N., Riccardi, G., 2017. Potential increase in coastal wetland vulnerability to sea-level rise suggested by considering hydrodynamic attenuation effects. Nat. Commun. 8, 16094.
Ross, A.C., Najjar, R.G., Li, M., Lee, S.B., Zhang, F., Liu, W., 2017. Fingerprints of sea level rise on changing tides in the Chesapeake and Delaware bays. J. Geophys. Res.: Oceans 122, 8102–8125.
Sadat-Noori, M., Santos, I.R., Tait, D.R., McMahon, A., Kadel, S., Maher, D.T., 2016. Intermittently Closed and Open Lakes and/or Lagoons (ICOLLs) as groundwater-dominated coastal systems: evidence from seasonal radon observations. J. Hydrol. 535, 612–624.
Savenije, H.H., 2006. Salinity and Tides in Alluvial Estuaries. Elsevier.
Speer, P.E., Aubrey, D.G., 1985. A study of non-linear tidal propagation in shallow inlet/estuarine systems Part II: theory. Estuarine. Coastal and Shelf Science 21, 207–224.
Strauss, B.H., Ziemlinski, R., Weiss, J.L., Overpeck, J.T., 2012. Tidally adjusted estimates of topographic vulnerability to sea level rise and flooding for the contiguous United States. Environ. Res. Lett. 7, 014033.
Swart, H.E.d., Zimmerman, J.T.F., 2009. Morphodynamics of tidal inlet systems. Annu. Rev. Fluid Mech. 41, 203–229.
Sweet, W.V., Kopp, R.E., Weaver, C.P., Obeysekera, J., Horton, R.M., Thieler, E.R., Zervas, C., 2017. In: Global and Regional Sea Level Rise Scenarios for the United States, 083), N.C.-O.
Talke, S.A., Jay, D.A., 2020. Changing tides: the role of natural and anthropogenic factors. Annual Review of Marine Science 12 null.
Tang, H.S., Kraatz, S., Qu, K., Chen, G.Q., Aboobaker, N., Jiang, C.B., 2014. High-resolution survey of tidal energy towards power generation and influence of sea-level-rise: a case study at coast of New Jersey, USA. Renew. Sustain. Energy Rev. 32, 960–982.
Titus, J.G., Richman, C., 2001. Maps of lands vulnerable to sea level rise: modeled elevations along the US Atlantic and Gulf coasts. Clim. Res. 18, 205–228.
van Maren, D.S., Winterwerp, J.C., Vroom, J., 2015. Fine sediment transport into the hyper-turbid lower Ems River: the role of channel deepening and sediment-induced drag reduction. Ocean Dynam. 65, 589–605.
van Rijn, L.C., 2011. Analytical and numerical analysis of tides and salinities in estuaries; part I: tidal wave propagation in convergent estuaries. Ocean Dynam. 61, 1719–1741.
Wiegman, A.R.H., Day, J.W., D'Elia, C.F., Rutherford, J.S., Morris, J.T., Roy, E.D., Lane, R.R., Dismukes, D.E., Snyder, B.F., 2018. Modeling impacts of sea-level rise, oil price, and management strategy on the costs of sustaining Mississippi delta marshes with hydraulic dredging. Sci. Total Environ. 618, 1547–1559.
Winterwerp, J.C., 2011. Fine sediment transport by tidal asymmetry in the high-concentrated Ems River: indications for a regime shift in response to channel deepening. Ocean Dynam. 61, 203–215.
Ye, F., Zhang, Y.J., Friedrichs, M.A.M., Wang, H.V., Irby, I.D., Shen, J., Wang, Z., 2016. A 3D, cross-scale, baroclinic model with implicit vertical transport for the Upper Chesapeake Bay and its tributaries. Ocean Model. 107, 82–96.
Young, S., Couriel, E., Jayewardene, I., McPherson, B., Dooley, B., 2014. Case study: assessment of the entrance stability of the Lake Illawarra estuary. Aust. J. Civ. Eng. 12, 41–52.
Yu, Q., Wang, Y., Gao, J., Gao, S., Flemming, B., 2014. Turbidity maximum formation in a well-mixed macrotidal estuary: the role of tidal pumping. J. Geophys. Res.: Oceans 119, 7705–7724.
Yuan, R., Zhu, J., 2015. The effects of dredging on tidal range and saltwater intrusion in the Pearl River Estuary. J. Coast Res. 31, 1357–1362.
Zhang, Y.J., Ye, F., Stanev, E.V., Grashorn, S., 2016. Seamless cross-scale modeling with SCHISM. Ocean Model. 102, 64–81.